CONCLUDING REPORT OF FLIGHT TEST DATA ANALYSIS ON THE SUPERSONIC EXPERIMENTAL AIRPLANE OF NEXST PROGRAM BY JAXA

Kenji YOSHIDA, Dong-Youn KWAK, Naoko TOKUGAWA, Hiroaki ISHIKAWA*
Japan Aerospace Exploration Agency, 6-13-1, Osawa, Mitaka, Tokyo, 181-0015, Japan
***Sankosoft Company, Ltd., Shinjuku, Tokyo, 169-0075, Japan**

Abstract

In the National EXperimental Supersonic Transport (NEXST) program by JAXA, a CFD-based inverse design technology to reduce airframe drag at supersonic speed was developed by applying an original design concept of natural laminar flow wing including well-known pressure drag reduction concepts. An unmanned and scaled supersonic experimental vehicle without propulsion system called "NEXST-1" was designed and manufactured to validate those design concepts and its flight test was successfully conducted on 10 October, 2005. Although principal results of preliminary analysis of the flight test data were already reported, JAXA continued to analyze whole data in detail for about three years after the flight test. This paper provides principal results of final analysis of the flight test data.

1 Introduction

Japan Aerospace Exploration Agency (JAXA) promoted National EXperimental Supersonic Transport (NEXST) program from 1997 to 2006, in order to develop an advanced aerodynamic design technology which will be required for a future international cooperative development of a next generation supersonic transport (SST) [1]. In this program, two CFD-based aerodynamic design techniques were developed for reducing aerodynamic drag at supersonic speed and some flight tests were planned to validate them using two types of an unmanned and scaled supersonic experimental vehicles.

The first vehicle, "NEXST-1" was a pure aerodynamic configuration without propulsion system to validate JAXA's advanced airframe drag reduction concept at supersonic speed. This vehicle was designed using an originally developed CFD-based inverse design method incorporating well-known pressure drag reduction concepts and a friction drag reduction concept. The latter is supersonic natural laminar flow (NLF) wing design concept [2, 3]. This vehicle was launched and inserted to the flight test condition by a solid rocket booster.

The second vehicle, "NEXST-2" was an aerodynamically designed airframe/nacelle configuration with twin jet engines. The main design concept was an original non-axisymmetrical area-ruled body design concept [2, 3, 4] to reduce interference drag between the airframe and two engine nacelles. The CFD-based optimum design method consisted of Euler analysis with overset grid system and application of "adjoint technique" for sensitivity analysis of design variables.

The first flight test of the NEXST-1 was conducted on 14 July 2002, but it was failed because of premature separation of the booster due to an electrical short in the firing system of separation bolts. This resulted in the freezing and ultimate cancellation of the NEXST-2 project, and all efforts were poured into improving and redesigning the NEXST-1 airplane system for second flight test. About three years later, the second flight test was successfully conducted on 10 October, 2005 and a lot of aerodynamic data were obtained [1].

Principal results of preliminary analysis of the flight test data was presented at both AIAA [5, 6] and ICAS [1, 7, 8] in 2006. By comparing the flight test ("FLT") data with CFD analysis results, JAXA's design concepts of reducing airframe drag at supersonic speed was qualitatively validated. However, there were a

few quantitative discrepancies between FLT and CFD data, for example zero-lift angle of attack and minimum drag. Therefore they had to be investigated further according to the following subjects:

1) Detail analysis of elastic deformation
2) Detail analysis of transition data
3) Re-consideration of measurement error
4) CFD analysis with measured laminar region
5) Verification of the NEXST-1 contour
6) Verification of accuracy of Air Data System
7) Investigation of turbulence model effect
8) Investigation of drag caused by small parts
9) Analysis of flight test data below Mach 2.0

JAXA studied these subjects to clarify physical reasons of those discrepancies and completed them in 2008.

The main objective of this paper is to provide principal results of final analysis of the flight test data. They are described in third section, also including an overview of the NEXST-1 program summarized in next section.

2 Overview of NEXST-1 Program

2.1 Aerodynamic Design of NEXST-1

Main target of the aerodynamic design of the NEXST-1 airplane was to reduce supersonic airframe drag. Firstly, a CFD-based inverse design technique was developed including both pressure and friction drag reduction concepts. Those design concepts were an arrow planform, warped wing (optimum cambered and twisted wing), area-ruled body, and natural laminar flow (NLF) wing. The application of NLF wing design concept to SST configurations with subsonic leading edge was the first application in the world.

To design the NLF wing, an ideal and optimum pressure distribution over the wing had to be derived as design target. JAXA investigated several pressure distributions using current e^N method and found the most effective pressure distribution. Then, the NEXST-1 airplane was designed and developed using the inverse design method as shown in Fig.1 [2, 3].

Before the flight test, JAXA also conducted a wind tunnel test to validate the effect of the NLF wing design concept. A circuit-type supersonic wind tunnel facility of ONERA (S2MA) was chosen for its low freestream disturbance. The concept was qualitatively confirmed but not quantitatively because of nonzero freestream disturbance [9].

In manufacturing the NEXST-1 airplane, its elastic deformation was carefully considered. This deformation was estimated by NASTRAN code, using inertial and aerodynamic loads at the design point which was Mach number M=2.0, lift coefficient C_L=0.1, and flight altitude H=18km. At first, jig shape (indicated as “JS”) used for manufacturing the NEXST-1 airplane was defined by subtracting its elastic deformation from the designed aerodynamic shape (“AS”). Then each elastically deformed shape (“ES”) with aerodynamic load at each flight test condition was estimated from the JS.

Furthermore, present actual flight vehicle had some additional small parts such as a camera, Air Data Sensor (ADS) probe, total temperature (TAT) sensor. And severe criterion for surface smoothness condition (averaged smoothness value of 0.3 micron meter in “Ra-metric”) was specified to detect transition at flight test condition.

The detail explanation of those design concepts, design process and principal design results are described in Ref.3.

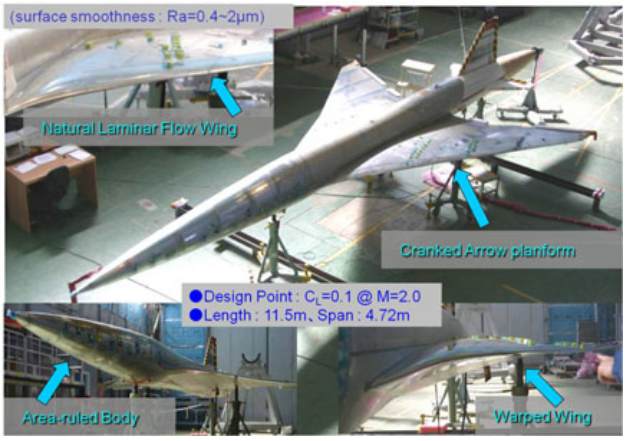

Fig.1 NEXST-1 airplane

2.2 Flight Test Plan and Aerodynamic Measurement System

(1) Flight test plan

In the flight test of the NEXST-1 airplane, two aerodynamic measurement phases were planned as demonstrated in Fig.2. One was an angle of

attack (AOA) sweep test phase around 18km altitude to obtain the airplane's drag characteristics. Another was an altitude sweep test phase while maintaining lift coefficient at the design value C_L=0.1. This corresponds to the Reynolds number (Re) sweep test phase to investigate the effect of NLF wing concept at higher Reynolds numbers than that at the design point. Since the NEXST-1 airplane was essentially a supersonic glider, it was impossible to precisely maintain the prescribed Mach number during the AOA sweep test, and tolerance of flight Mach number was therefore specified as 0.05 (namely from M=1.95 to 2.05) considering wind tunnel test results [1, 3].

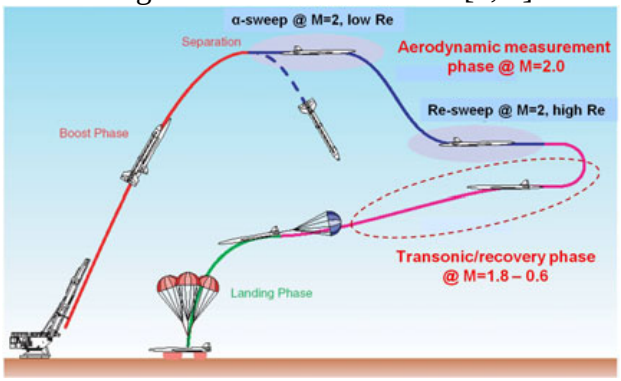

Fig.2 Flight test plan

(2) Force and moment measurement system

Three-axis forces and moments were measured using momentum balance equations and six acceleration values measured with inertial measurement unit (IMU) placed near the center of gravity of the NEXST-1 airplane. Fig.3 shows a procedure and method to detect forces and moments. In general, some measurement errors exist in the process of measurement system which consists of data analysis software and hardware [3]. According to the precision of several measurement components, the measurement error bars of lift (C_L), drag (C_D), and pitching moment (C_m) were predicted using root sum square (RSS) rule as $\Delta C_L = \pm 0.00064$, $\Delta C_D = \pm 0.00020$, and $\Delta C_m = \pm 0.00152$.

(3) Surface Pressure Measurement System

Surface pressure distributions were measured using seven differential type pressure scanners and one absolute type pressure transducer for measuring back-pressures of each sensor of the scanners. 322 pressure holes were placed on the right wing and body as shown in Fig.4. Maximum measurement error was also predicted as $\Delta P = \pm 244$Pa and $\Delta Cp = \pm 0.0115$ at the condition of altitude 18km [5].

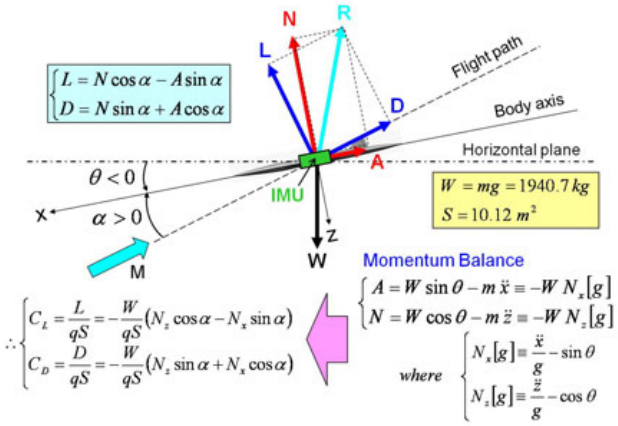

Fig.3 Procedure of estimating lift and drag

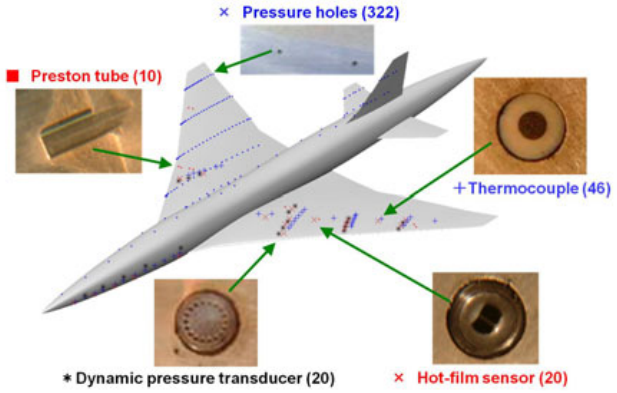

Fig.4 Aerodynamic measurement sensors

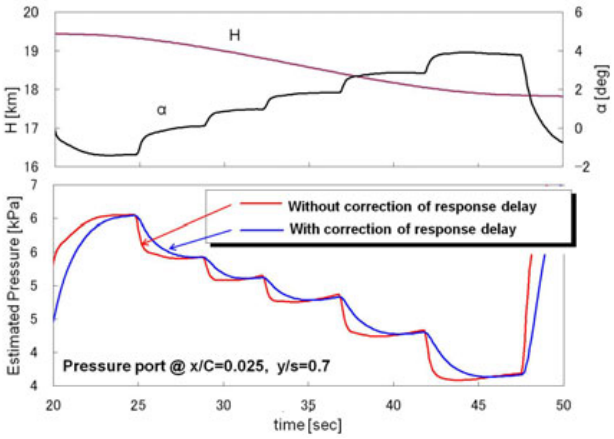

Fig.5 Response delay of pressure measurement system

In this measurement system, the correction for the response delay in propagating pressure at high altitude was carefully considered because of long and slender tubes. At first, JAXA investigated whole delay time of each pressure tube using an empirical relation, which was validated using an original wind tunnel test.

Then, to neglect the response delay, flight test condition was improved by using so-called "pitch and pause" change of AOA. According to this analysis, about four seconds were enough for keeping a pause state until neglecting the difference between true and delayed pressure values as shown in Fig.5. As a result, six AOA steps were finally chosen to obtain a polar curve during Mach number 2.0 [5].

(4) Transition Measurement System

To increase the possibility of transition detection, the following four kinds of detection techniques were applied: hot-film sensors (HF), dynamic pressure transducers (DP), Preston tubes (Pr), and thermocouple sensors (TC). These sensors were placed on the wing and left side of the front body as shown in Fig.4. To obtain the correlation of each transition detection technique, JAXA conducted a wind tunnel test to measure transition phenomenon using a nose cone model incorporated with those sensors. Fig.6 shows a summary of the test, in which good correlation among whole sensors was definitely obtained [10].

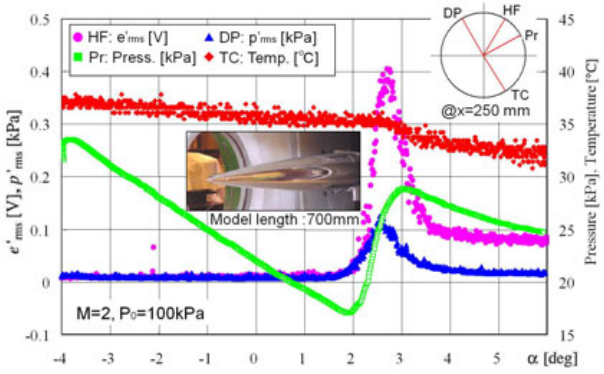

Fig.6 Correlation of four types of transition sensors

3 Analysis of Flight Test Data

3.1 Flight Test Conditions

Fig.7 shows actual flight trajectory with photographs. The achieved trajectory was almost the same as predicted, with the vehicle well controlled by its onboard flight computer to realize the prescribed lift condition [7].

In the AOA sweep test phase, each C_L value was definitely controlled to be -0.01, 0.04, 0.07, 0.10, 0.14, and 0.17 corresponding to six AOA steps respectively. The design C_L condition was achieved at the 4th step. Flight altitude varied from 18.9 to 17.5 km and the Reynolds number based on the mean aerodynamic chord (MAC) of 2.754 m varied from 12.7 to 15.8 million.

In the Re sweep test phase, C_L of the vehicle was kept to be the design value of 0.1 during the variation of flight altitude from 12.2 to 11.5 km corresponding to the variation of the Reynolds number based on MAC from 34.3 to 34.7. Although only a narrow range of Reynolds number was achieved, the effect of Reynolds number sweep was estimated by comparing the result at the 4th step of the AOA sweep test (α _4) with that at the Re sweep test.

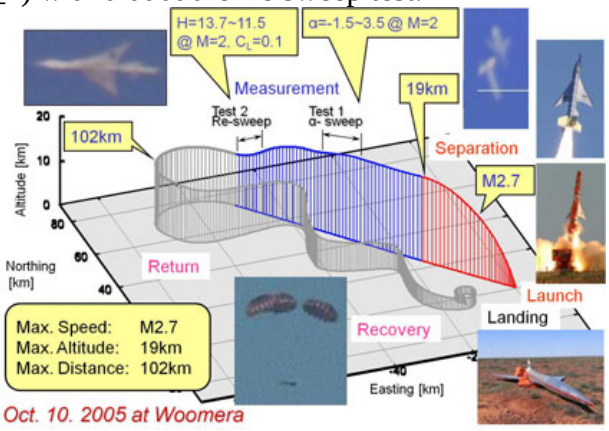

Fig.7 Flight test sequence and trajectory

Here, some of flight test conditions such as Mach number (M), angle of attack (AOA), and slid slip angle (SSA) were measured by the ADS probe as indicated in Fig.8(a). As for the probe, four static pressures on each four face of its pyramid-type shape and one total pressure at center were measured. Then M, AOA, and SSA were calculated from these five measured pressures using a data map which was based on precise correlation data obtained by some wind tunnel tests in the development of the NEXST-1 airplane. The measurement error bar of M and AOA, namely Δ M and Δ AOA were also predicted to be 0.01 and 0.014 degrees respectively according to the map.

In final analysis phase of the flight test data, JAXA confirmed the validity of the data map again, and improved its precision by the same wind tunnel test as previous one. And Reynolds number effect on the map was also investigated

by using CFD analysis. Detail configuration of the ADS probe for grid generation and a typical result is demonstrated in Fig.8(c). Then, JAXA confirmed no remarkable Reynolds number effect on the map [13].

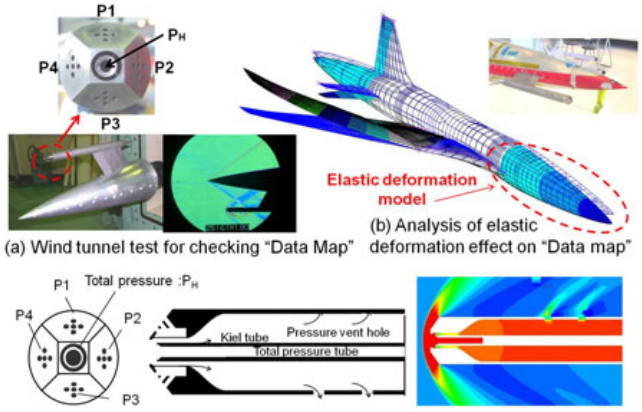

Fig.8 Correction items for ADS data

Furthermore, elastic deformation of the front nose had strong influence on the correction of measured AOA values. According to a precise analysis model [14] for the elastic deformation of the body as demonstrated in Fig.8(b), additional deflection angle to reference line of the IMU was estimated to be $\Delta\theta$ =0.072[degree/G] × Nz[G]. Therefore, JAXA corrected each measured AOA value due to the ADS probe using this relation with measured Nz value at each flight test condition.

After those aerodynamic measurement phases at M=2, the NEXST-1 airplane flew at lower supersonic speed than 2.0, then it slowed down for recovery from transonic to subsonic speeds. This flight achieved the flight condition of scheduled combination of M and AOA. Present aerodynamic measurement system also provided force and moment data except transition data, because of no expectation of laminarization except the design M and AOA. Although surface pressures were measured, they included large response delay [5].

Finally, those flight test conditions including C_L, C_D, and C_m data are summarized in Table 1. Particularly, a trend of measured M and AOA are demonstrated in Fig.9 [15].

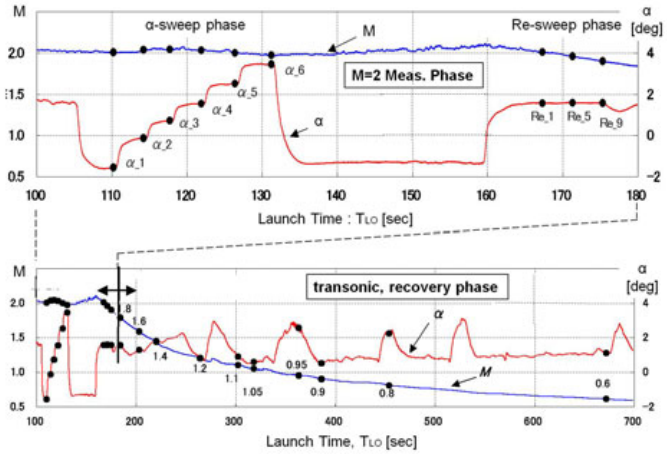

Fig.9 Flight test conditions

Table 1 Flight test conditions and force data

Phase		TLO[sec]	M	α [deg]	β [deg]	H[km]	T∞[K]	Q[kPa]	Re[million] based on MAC	CL	CD	Cm
α-sweep phase	α1	110.22	2.00	-1.57	-0.08	18.94	206.35	18.19	12.72	-0.0103	0.0105	0.0062
	α2	114.22	2.04	-0.14	-0.14	18.91	201.87	18.85	13.37	0.0400	0.0105	-0.0104
	α3	117.72	2.04	0.71	-0.01	18.51	202.27	20.18	14.25	0.0709	0.0117	-0.0203
	α4	121.92	2.03	1.53	-0.08	18.10	204.09	21.30	14.93	0.1020	0.0135	-0.0302
	α5	126.43	2.00	2.51	-0.08	17.68	205.79	22.08	15.54	0.1372	0.0168	-0.0413
	α6	131.25	1.97	3.44	0.00	17.47	205.65	22.15	15.84	0.1714	0.0209	-0.0522
Re-sweep phase	Re1	167.35	2.01	1.56	-0.08	12.24	217.22	52.59	34.25	0.0995	0.0133	-0.0293
	Re5	171.35	1.96	1.58	-0.15	11.69	222.95	54.44	35.15	0.1010	0.0134	-0.0296
	Re9	175.33	1.90	1.56	-0.18	11.45	226.29	53.18	34.70	0.1016	0.0135	-0.0297
Transonic & Recovery phase	1.8	184.10	1.79	1.56	-0.43	11.68	225.91	45.57	31.62	0.1113	0.01376	-0.0323
	1.6	203.20	1.59	1.29	-0.64	12.58	219.18	31.07	25.31	0.1078	0.01353	-0.0293
	1.4	220.18	1.44	1.80	-0.47	12.91	217.82	24.20	21.94	0.1352	0.01553	-0.0370
	1.2	264.28	1.21	0.81	-0.44	12.21	219.97	19.08	20.33	0.0986	0.01350	-0.0228
	1.1	302.36	1.10	0.90	-0.36	10.98	227.31	19.31	21.58	0.1039	0.01391	-0.0241
	1.05	318.34	1.05	0.58	-0.36	10.53	230.19	18.78	21.70	0.0882	0.01345	-0.0192
	0.95	363.48	0.95	2.55	-0.21	8.90	237.70	19.75	24.11	0.2009	0.01683	-0.0504
	0.9	386.21	0.90	0.51	-0.56	8.42	240.54	18.99	24.11	0.0762	0.00850	-0.0120
	0.8	454.01	0.81	2.24	-0.22	6.78	248.98	19.40	26.20	0.1541	0.01282	-0.0299
	0.6	672.00	0.61	1.10	-0.43	2.44	278.52	19.65	30.39	0.0913	0.00908	-0.0134

3.2 Surface Pressure Data Analysis

In the preliminary analysis, JAXA already found that elastic deformation was the most important correction item to investigate the discrepancy between measured and CFD-based Cp distributions [3, 5]. To increase the accuracy of elastic deformation analysis, JAXA investigated it by using both CFD and NASTRAN with a more precise polygon-type model than a previous plate-type model as shown in Fig.10 [14].

At the design point (α _4), the elastically deformed configuration ("ES") was almost same as the aerodynamically designed configuration ("AS") as shown later (in Fig.12). However, at other flight test conditions, significant differences between the ES and AS were obtained. Especially, at the condition of higher AOA or higher Reynolds number than that at the design point, large upward displacement at tip and down-twist were predicted as shown in Fig.10. Also, present analysis was validated by comparing predicted results (indicated as "ES") with FLT data measured by strain-gauge sensors of the wing as shown by "FLT" in Fig.10 [14].

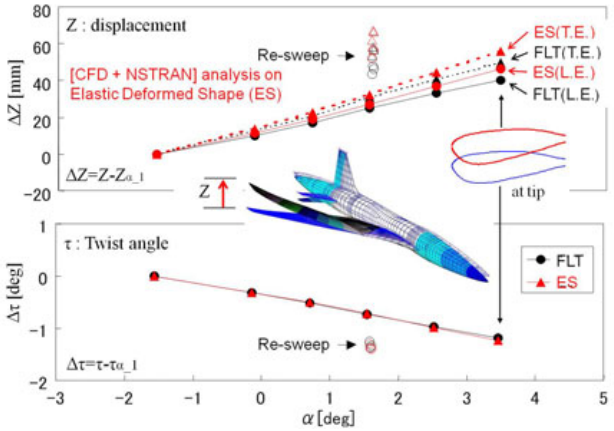

Fig.10 Elastic deformation analysis and validation

Based on reconsideration of the flight test conditions and precise analysis of elastic deformation of the wing and body, JAXA conducted CFD analysis for the ES again. Fig.11 shows comparison between measured and CFD-based pressure coefficient (Cp) distributions on the wing at the design condition (α _4) [11, 15]. Especially, high correlation between them on the upper surface was confirmed within the measurement error of Δ Cp=$\pm$0.0115 (demonstrated as symbol of "I"). This indicates necessary condition for the NLF wing was satisfied in the flight test.

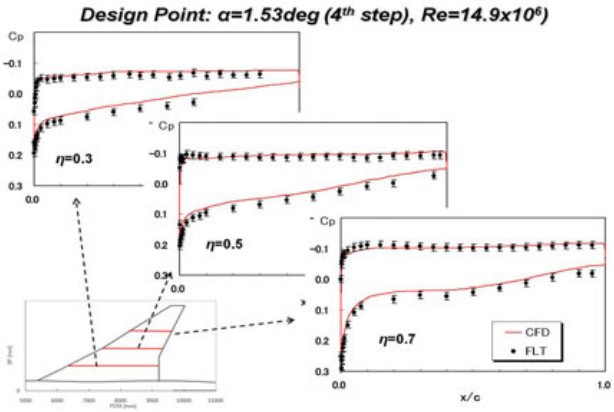

Fig.11 Comparison of Cp distributions at design point

However, a slight difference of the lower surface Cp distributions between flight test and CFD analysis was still remained. Since its elastic deformation effect was already included enough, investigation of actual contour of the NEXST-1 airplane was conducted using 3-D contour measurement system. However, no meaningful error was found. Therefore, no effective reason to explain such discrepancy has been clarified. This is still an open subject. However, JAXA concluded this discrepancy was not too large from the viewpoint of practical application of the design concept.

In order to clarify the effect of elastic deformation, Fig.12 shows the comparison of CFD-based Cp distributions near tip region between the AS and ES. At the design condition (α _4), effectiveness of the JS design was definitely confirmed because any remarkable difference of both Cp distributions was not observed. Of course, there were remarkable differences apart from the design condition. From the comparison of Cp distributions at α _4 and α _6, elastic deformation shows a slight reduction of local AOA. The comparison of Cp distributions at α _4 and Re_5 (indicated in Table 1) shows similar effect to the case at higher AOA because the increase of dynamic pressure at Re_5 generates larger elastic deformation [14]. These comparisons between measured and CFD-based Cp distributions are summarized in Fig.A-1 of Appendix A.

Finally, as for the comparison of Cp distributions on the body, high correlation between FLT and CFD results was also obtained as shown by " η =0" in Fig.A-1. Therefore, JAXA concluded that it demonstrated an important evidence to validate the area-ruled body design concept.

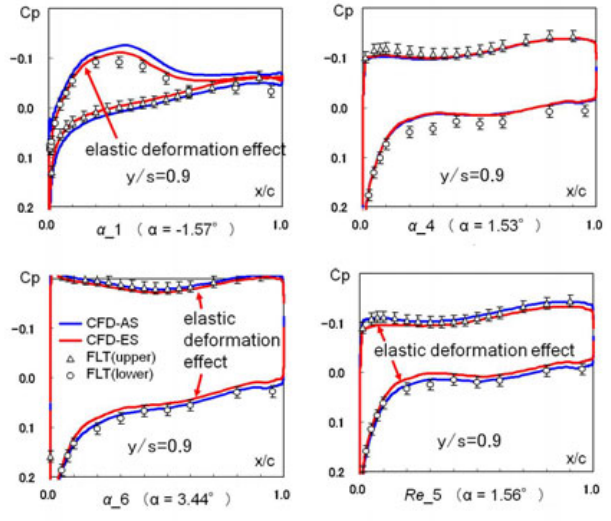

Fig.12 Effect of elastic deformation on Cp distributions

3.3 Transition Data Analysis

After the preliminary analysis, JAXA continued to analyze measured transition data more precisely. First of all, whole time histories of measured signals of all transition detection sensors were investigated in detail. Using the correlation of four types of transition sensors and the comparison of their waveforms, it was carefully judged whether the state of boundary layer was laminar or turbulent.

Fig.13 shows a time history of measured signals of representative HF sensor [HF]. This figure includes both DC[mean] and AC[rms] signals and typical waveform. According to those data, the state of boundary layer was roughly judged to be laminar or turbulent as demonstrated in the figure [6, 8]. Some similar time histories of other representative sensors are summarized in Fig.B-1 of the Appendix B.

Then, JAXA conducted detail investigation to make quantitative judgment of the boundary layer state. As a new approach, an index of transition level was introduced in analyzing measured data. Fig.14 shows an example of the relation of transition level to the AC[rms] signal of a HF sensor. Present transition levels are defined from level 1-2 (fully laminar) to 6-7 (fully turbulent), with transition process occupying levels 3-5 [10].

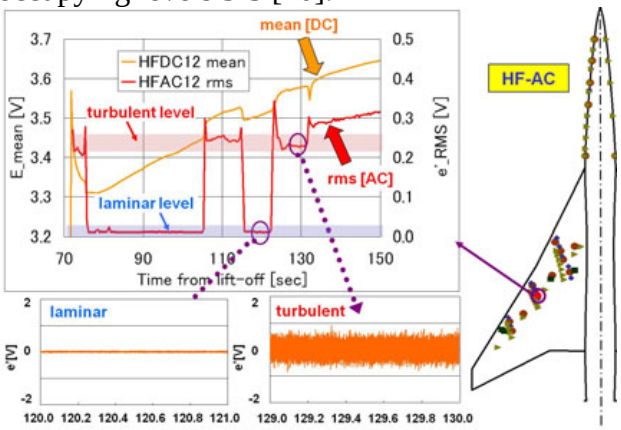

Fig.13 Time history of HF signals

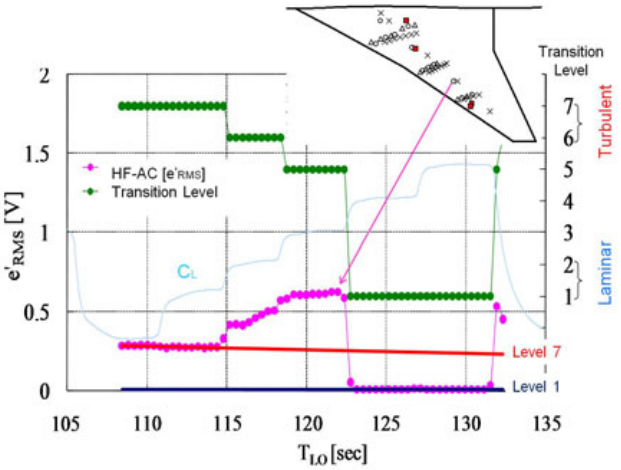

Fig.14 Definition of transition level for HF-AC signals

According to present judgment based on transition level, the transition pattern in the preliminary analysis phase was quantitatively improved. To make clear of the NLF effect, namely friction drag reduction effect, the boundary between turbulent and non-turbulent regions is useful and effective. The whole transition patterns defined as the boundary at each flight test condition are summarized in Figs.B-2(a)-2(g) of Appendix B.

Fig.15 shows the comparison of measured transition pattern and JAXA's transition analysis results [12]. This method consists of both computations of laminar boundary layer profiles and their stability characteristics. It was originally developed by JAXA in the aerodynamic design phase of the NEXST-1 airplane and improved with application of NS

computations for laminar boundary layer profiles after the flight test [12].

In the transition prediction based on this method, one parameter related to transition, namely "N" must be specified as transition criterion. However, any database for a reliable N value related to transition in supersonic flow has not been made in the world yet. Therefore, JAXA expected present transition detection data were very useful and effective to advance the transition prediction method.

Fig.15 shows the comparison of predicted transition lines based on the assumed N values and measured transition pattern at the design condition. Unfortunately, high correlation between them over the whole wing was not obtained, but the line of N=11 had almost good correlation with measured transition pattern at inner wing region [12]. As for the outer wing region, there may be a possibility of influence of surface roughness because boundary layer was thinner than the inner wing region. The surface roughness was measured before and after the flight test, and it was about 1 micron meter in "Ra-metric". This value is larger than the target level (Ra=0.3 micron meter) in the design process of the NEXST-1 airplane.

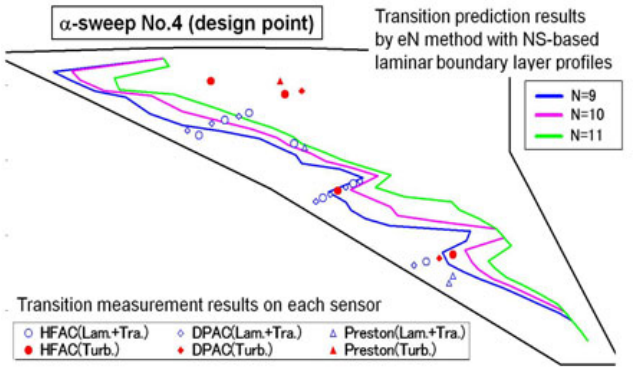

Fig.15 Comparison of measured transition with prediction

Furthermore, a comparison of transition pattern at α_4 and Re_5 as shown in Figs.B-2(d) and B-2(g) of Appendix B demonstrates remarkable roughness effect, because laminar region is much narrower than predicted one. In general, it is not easy to analyze surface roughness effect. Therefore, JAXA expects the present measured transition data are useful to promote such a research subject.

3.4 Force Data Analysis

As mentioned in "Introduction", some remarkable differences in zero-lift AOA (α_0) and minimum drag (C_{Dmin}) were mainly obtained. The following corrections were investigated further in the final data analysis phase.

- For measurement data :
  a. ADS measurement values: corrected by new data map
  b. AOA of ADS: corrected by elastic deformation effect of the front nose
  c. Influence of nonzero SSA and some deflection angles of control surfaces: corrected by wind tunnel test data at the development of the NEXST-1 airplane
- For CFD data [11, 13, 14]:
  a. CFD code: validated by comparing CFD results with new wind tunnel test results
  b. Elastic deformation effect: corrected by CFD analysis on the ES
  c. Influence of some additional small parts on C_{Dmin}: corrected by a certain combination of new wind tunnel test (WTT) results and CFD analysis results on them (Principal results of them are summarized in Fig.16 [11].)
  d. NLF wing effect: corrected by CFD analysis with measured laminar region (Principal results are summarized in Fig.17.)
  e. Effect of turbulence model: corrected by considering the difference between Sparat-Allmaras (SA) model and Menter's shear stress transport (SST) model

According to the procedure shown in Fig.3 and several results mentioned above, lift, drag, and pitching moment characteristics at the flight test conditions are summarized in Figs.18-20.

These figures also include CFD results which were newly computed under the following conditions:

- CFD code: JAXA's UPACS code
- grid: structured grid
- configuration : ES
- boundary layer: measured transition pattern as shown in Fig.B-2(a)-B-2(f)

- turbulence model: SA model
- Assumption 1: no side slip angle (SSA) of the vehicle and no deflection angles of any control surfaces, because some influences due to them were already corrected for the flight test data to be compared.
- Assumption 2: minimum drag increment of 7 counts due to small parts, which was derived as an averaged value of wind tunnel test and CFD analysis results on the AS with small parts as shown in Fig.16.
- Assumption 3: minimum drag reduction of 4 counts estimated by applying the drag reduction at the design condition due to the change of turbulence model from SA model to SST model. (Although it is not clear whether this reduction is valid or not, this reduction shows one possibility to improve the discrepancy of C_{Dmin} between FLT and CFD data.)
- Assumption 4: maximum drag reduction of 5.3 counts at the design condition estimated by CFD analysis with measured laminar region, which corresponded to about 40% laminarization in average as shown in Fig.17.

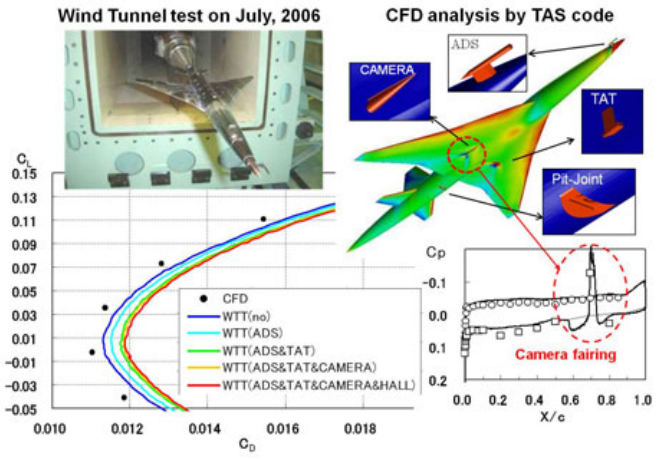

Fig.16 Influence of additional small parts on drag

Fig.18 shows the comparison of lift characteristics of flight test data indicated as “square symbol” and CFD analysis results indicated as “circle symbol”. First of all, lift slope $C_{L\alpha}$ of the flight test data agrees very well with the CFD result. However, the measured zero-lift angle α_0 had a slight offset of 0.24 degrees from the CFD results. This value was about twice of measurement error bar of the AOA. Although JAXA considers there is a certain mechanism to explain this offset, any reason for this discrepancy has not been clarified yet.

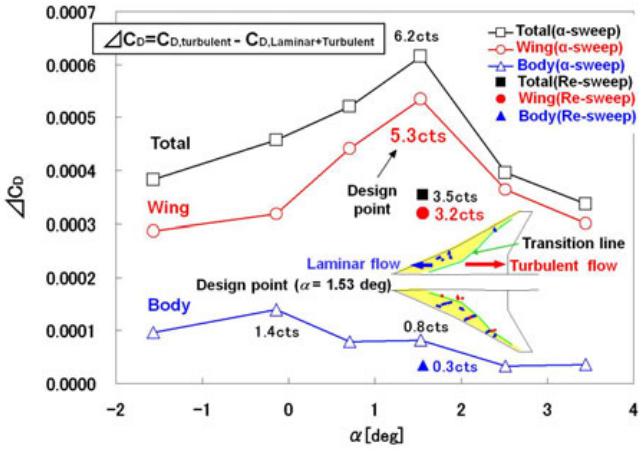

Fig.17 Influence of laminar region on drag

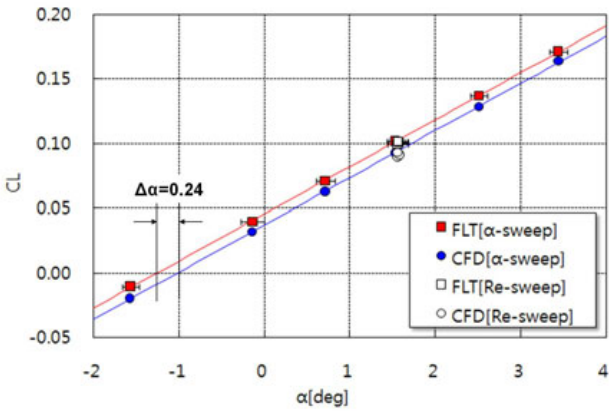

Fig.18 Lift characteristics

Drag characteristics are summarized in Fig. 19, comparing flight test data with present CFD analysis results. Here, in the preliminary analysis phase, JAXA assumed turbulent boundary layer at each flight test condition. As indicated above, JAXA considered the drag reduction effect in polar curve due to the extent of laminar region using fixed transition location conditions based on measured transition information.

Except for C_{Dmin}, the shape and vertical offset of both polar curves were very similar. In general, the shape of polar curve reflects planform effect, and the offset is generated by warp effect. Therefore, these high correlations indicate that present flight test validated both planform and warped wing design concepts for reducing lift-dependent drag.

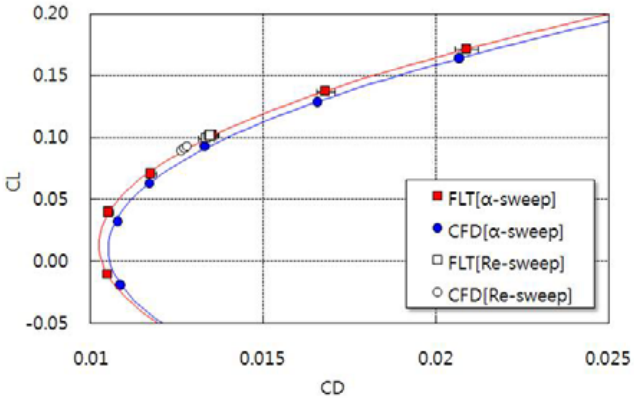

Fig.19 Drag characteristics

As for the validation of area-ruled body design concept, the amount of drag reduction effect is included in the C_{Dmin}, because this concept reduces wave drag due to volume, namely non-lift drag. Therefore, the concept is not directly validated by the comparison of both drag polar curves. As mentioned above, it was indirectly validated by comparing pressure distributions on the body between flight test data and CFD analysis results.

On the other hand, the difference of C_{Dmin} between them was finally reduced to about 3 counts from 6 counts in the preliminary analysis phase. However, this value is larger than measurement error bar. JAXA has considered there is a certain mechanism to explain it. In general, C_{Dmin} consists of friction drag and wave drag due to volume, and the former is strongly dominated by Reynolds number effect on turbulent friction drag. Present CFD analysis has some numerical errors, which were based on the four "Assumptions" mentioned above and inherent CFD errors due to its scheme, grid system, and so on. Therefore, it is not easy to increase the accuracy of estimating the C_{Dmin} quantitatively.

Fig.20 shows similar comparison on pitching moment characteristics. In this case, as moment characteristics are summarized in the change of lift, an offset such as α_0 was not found. However, there is remarkable difference of moment slope between FLT and CFD results. JAXA considered one of the principal reasons of the difference was the correction of lift of horizontal-tail due to the deflection angles of control surfaces. It was based on wind tunnel test data obtained by using a scaled tunnel model with deflected control surfaces. The accuracy of those data is not well investigated.

Furthermore, there is influence of elastic deformation of the rear body on pitching moment due to the horizontal tails (see Fig.8(b)). Therefore, JAXA has recognized further study from the viewpoint of aerodynamics. However, the differences between FLT and CFD data in α_0, C_{Dmin}, and C_m slope are approximately small. Therefore, JAXA concluded present comparison of FLT and CFD results demonstrated meaningful validation of the design concepts from the viewpoint of their practical application.

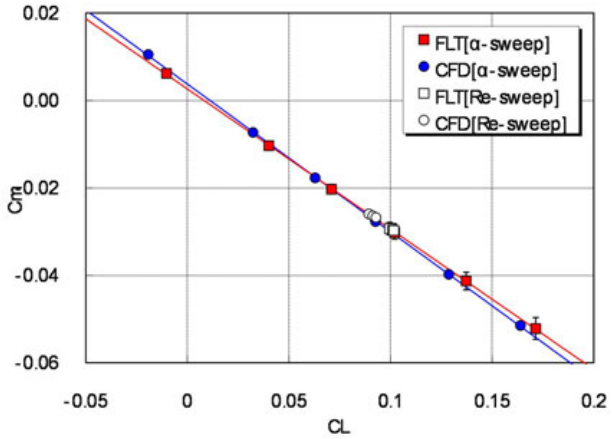

Fig.20 Pitching moment characteristics

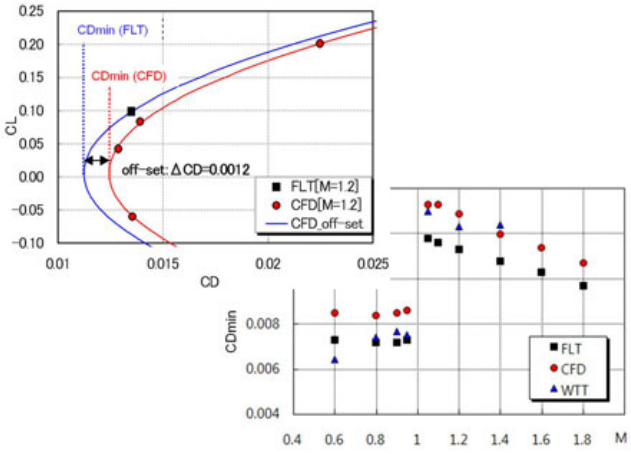

Fig.21 Drag characteristics at whole Mach range

Finally, although present flight test focused on aerodynamic measurement at the design Mach number condition, namely M=2.0, the NEXST-1 airplane had an ability to measure aerodynamic data at other flight test conditions shown in Table 1. However, a drag polar at fixed Mach number was not able to be obtained,

because of lack of AOA sweep phase. Therefore, each measured force value at each Mach number was compared with a CFD-based polar curve. Then, JAXA estimated the minimum drag C_{Dmin} approximately by using the CFD-based polar curve with a shift of the difference between measured and CFD-based C_D as shown in Fig.21 [15]. This comparison data is expected to be useful and effective to validate any CFD analysis tools at flight test conditions.

3.5 Summary of Flight Test Results

The flight test results can be summarized as follows. The effects of the arrow planform and warped wing concepts were validated directly by the close agreement of both the lift slope and shape of polar curve between flight test and CFD analysis results. The effect of the NLF wing design concept was also validated by obtaining good agreement of Cp distributions on the wing between the flight test and CFD analysis, and the rearward movement of the transition location at the design condition as shown in Fig.15. The measured laminar region was estimated to be about 40% of the upper wing surface.

Furthermore, good agreement of fuselage Cp distribution between the flight test and CFD analysis probably validated the effect of the area-ruled design concept. However, a discrepancy between the measured and CFD-based C_{Dmin} indicated that it was difficult to validate the effect of the NLF wing design concept quantitatively and completely by the flight test, because it is difficult to estimate turbulent skin friction reliably by any turbulence models.

JAXA concluded that the flight test proved the drag reduction concepts. However, the effect of Reynolds number variation was not completely obtained, because there was certain surface roughness effect. This must be one of future research subjects by JAXA.

4 Evaluation of NEXST technology

At the final stage of NEXST-1 program, JAXA investigated the overall effectiveness of applying these concepts to a full-size SST configuration by comparing the effect of the NEXST-1 concepts with a representative “Reference” configuration corresponding to a first generation SST. For this comparison, JAXA designed two full-scale SSTs: the “Reference” configuration (Concorde-like configuration without nacelles) using usual aerodynamic design procedure referring to [16], and a full-scale configuration using NEXST-1 concepts. For the latter, 30% laminarization on the upper surface of a full-scale configuration was predicted if the new optimum pressure distribution originally derived for the NLF wing design at a higher Reynolds number condition was applied.

The principal results of this comparison are summarized in Fig.22. Applying the NEXST-1 design concepts improves the L/D by about 13% at the cruise condition compared with the “Reference” configuration, and improvement is also evident in the predicted drag polar curves shown in Fig.22 [3].

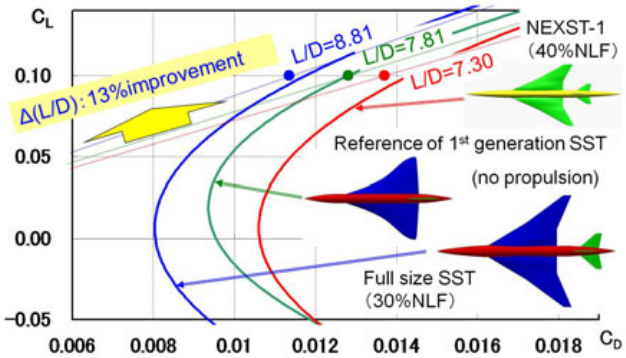

Fig.22 Effect of NEXST-1 concepts on a full-size SST

5 Concluding Remarks

JAXA developed CFD-based supersonic drag reduction techniques in the NEXST program. A supersonic NLF wing design concept and CFD-based inverse design procedure were newly developed. The NLF wing design concept was validated in the flight test by confirming actual delay of transition to about 40% local chord. Furthermore, the NEXST-1 aerodynamic design technique estimates to achieve L/D with about 13% greater than that with conventional design method for a 1st generation SST.

Finally, to complete the NEXST-1 design concepts, an airframe/propulsion interference drag reduction method must be incorporated.

JAXA already developed such a method and non-axisymmetrical area-ruled body design concept in the NEXST-2 program. JAXA has been challenging several fundamental research activities to improve the aerodynamic performance of a future SST.

Acknowledgement

The authors would like to express special thanks to Mitsubishi Heavy Industries (MHI), Kawasaki Heavy Industries (KHI), Fuji Heavy Industries (FHI) and Tohoku University for their cooperation in the aerodynamic designs of both NEXST airplanes. Furthermore, the authors also would like to thank several researchers of JAXA for their lots of research activities related to this program.

References

[1] Ohnuki T, Hirako K and Sakata K. National Experimental Supersonic Transport Project. ICAS2006-1.4.1, 2006.

[2] Yoshida K and Makino Y. Aerodynamic Design of Unmanned and Scaled Supersonic Experimental Airplane in Japan. ECCOMAS 2004, Jyva¨skyla¨, July 2004.

[3] Yoshida K. Supersonic drag reduction technology in the scaled supersonic experimental airplane project by JAXA. Progress in Aerospace Sciences, vol.45, pp.124-146, 2009.

[4] Makino Y, Iwamiya T and Lei Z. Fuselage shape optimization of a wing-body configuration with nacelles. Journal of Aircraft, Vol. 40, No.2, pp.297–302, 2003. [or AIAA-2001-2447, 2001].

[5] Kwak D.Y, Yoshida K, Ishikawa H and Noguchi M. Flight test measurements of surface pressure on unmanned scaled supersonic experimental airplane. AIAA-2006-3483, 2006.

[6] Tokugawa N and Yoshida K. Transition detection on supersonic natural laminar wing in the flight. AIAA-2006-3165, 2006.

[7] Fujiwara T, Hirako K and Ohnuki T. Flight plan and flight test results of experimental SST vehicle NEXST-1. ICAS2006-6.2.1, 2006.

[8] Tokugawa N, Kwak D.Y and Yoshida K. Transition measurement system of experimental supersonic transport—NEXST-1. ICAS2006-6.2.1, 2006.

[9] Sugiura H, Yoshida K, Tokugawa N, Takagi S and Nishizawa A. Transition measurements on the natural laminar flow wing at Mach 2. Journal of Aircraft, vol.39, No.6, pp.996–1002, 2002.

[10] Tokugawa N, Kwak D.Y, Yoshida K and Ueda Y. Transition measurement of natural laminar flow wing on supersonic experimental airplane NEXST-1. Journal of Aircraft, vol.45, No.5, pp.1495-504, 2008.

[11] Ishikawa H, Kwak D.Y and Yoshida K. Numerical Analysis on Flight-Test Results of Supersonic Experimental Airplane NEXST-1. Journal of Aircraft, vol.45, No.5, pp.1505-1513, 2008.

[12] Yoshida K, Sugiura H, Ueda Y, Ishikawa H, Tokugawa N, et al. Experimental and numerical research on boundary layer transition analysis at supersonic speed: JAXA-ONERA cooperative research project. JAXA-RR-08-007E, 2009.

[13] Ishikawa H, Kwak D.Y, Noguchi M and Kuroda F. Numerical Study of a Pitot Probe with Five-Hole Head for Supersonic Flight Test. ICAS2008-3.2.4.

[14] Kawakami H, Takatoya T and Ishikawa H. Static Aeroelastic Analysis of Experimental SST NEXST-1 Flight Test using Wing-Body Configuration Model. AIAA-2008-6419, 2008.

[15] Kwak D.Y, Ishikawa H and Yoshida K. Flight Test Results at Transonic Region on Supersonic Experimental Airplane (NEXST-1). ICAS2008-2.4.2, 2008.

[16] Rech J and Leyman C.S. A case study by Aerospatiale and British Aerospace on the Concorde. AIAA Professional Study Series, 1981.

Copyright Statement

Appendix A. Summary of Comparison of Pressure Distributions

Measured Cp distributions over the wing and body are summarized in Fig. A-1(a) to A-1(g) comparing with CFD data on the AS and ES.

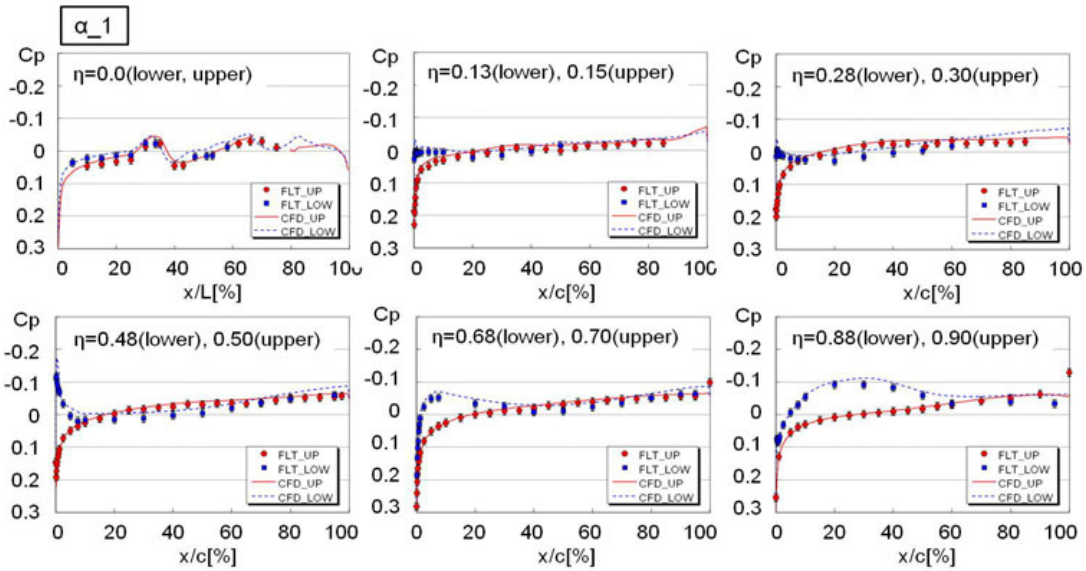

Fig.A-1(a) Comparison of Cp distributions at α _1

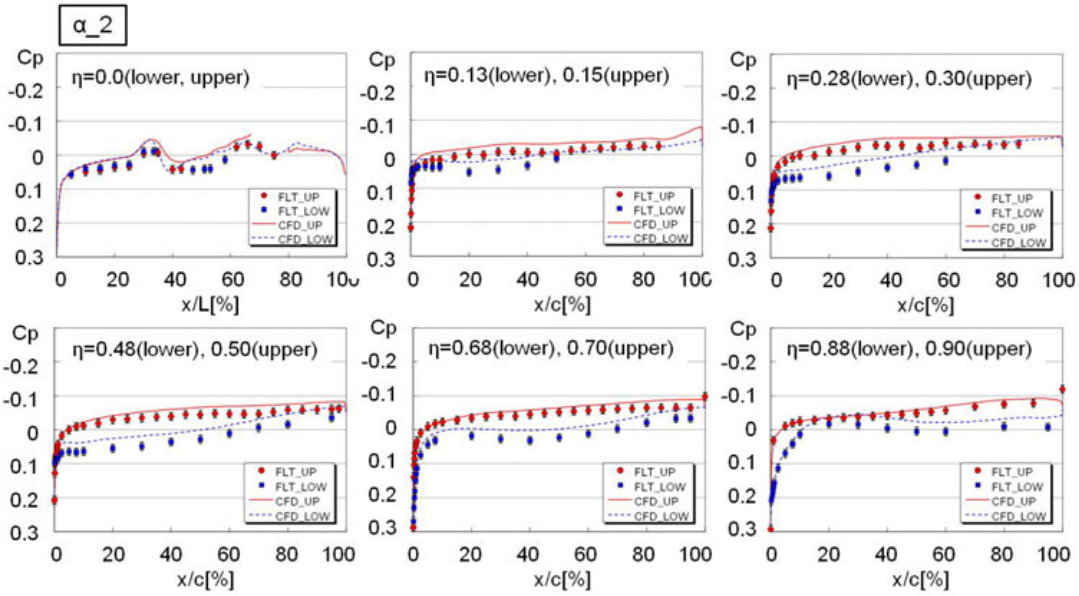

Fig.A-1(b) Comparison of Cp distributions at α _2

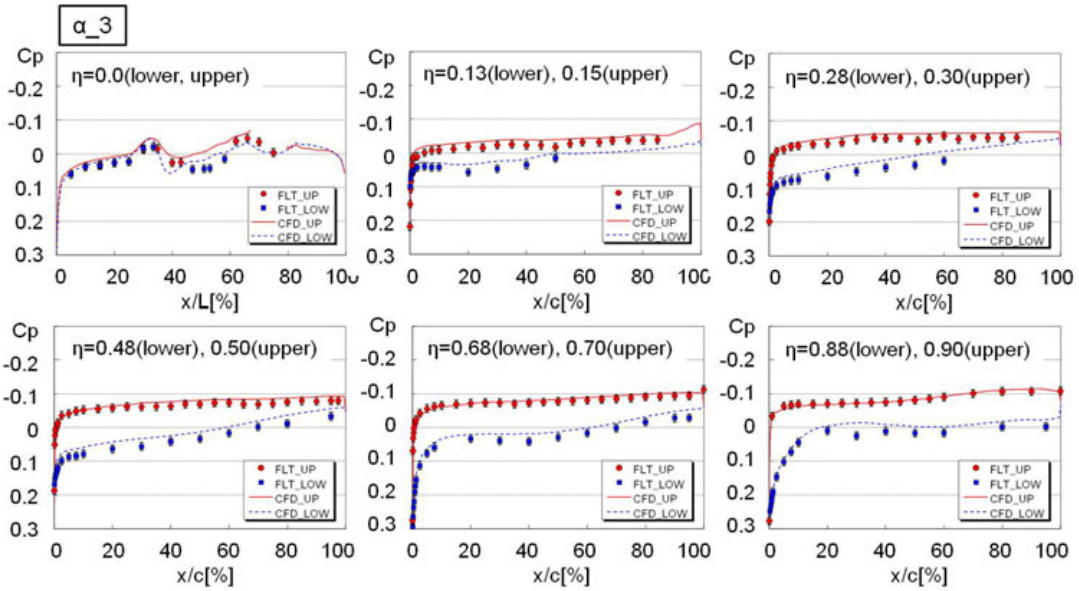

Fig.A-1(c) Comparison of Cp distributions at α _3

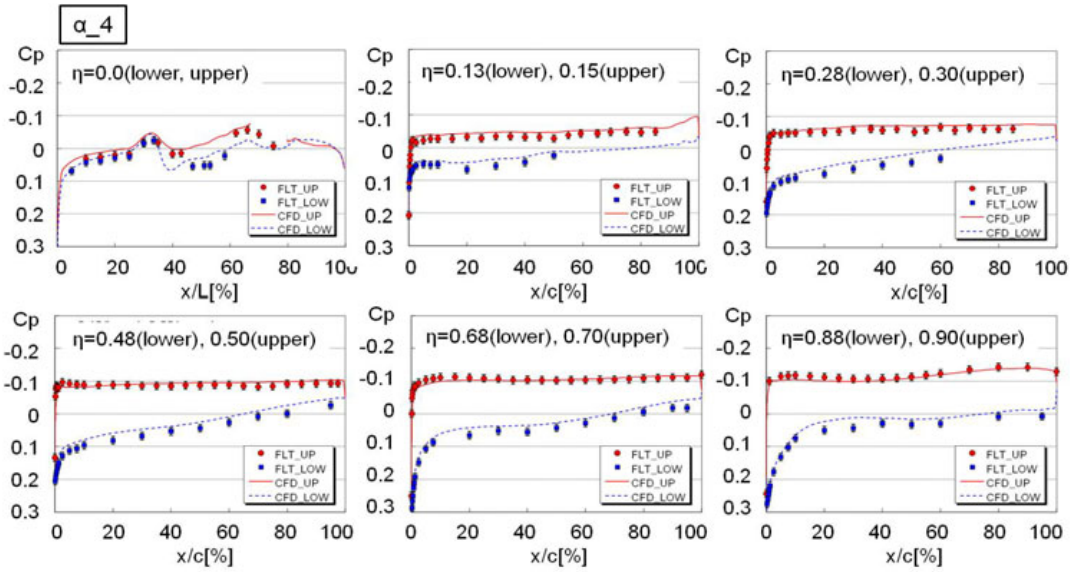

Fig.A-1(d) Comparison of Cp distributions at α _4

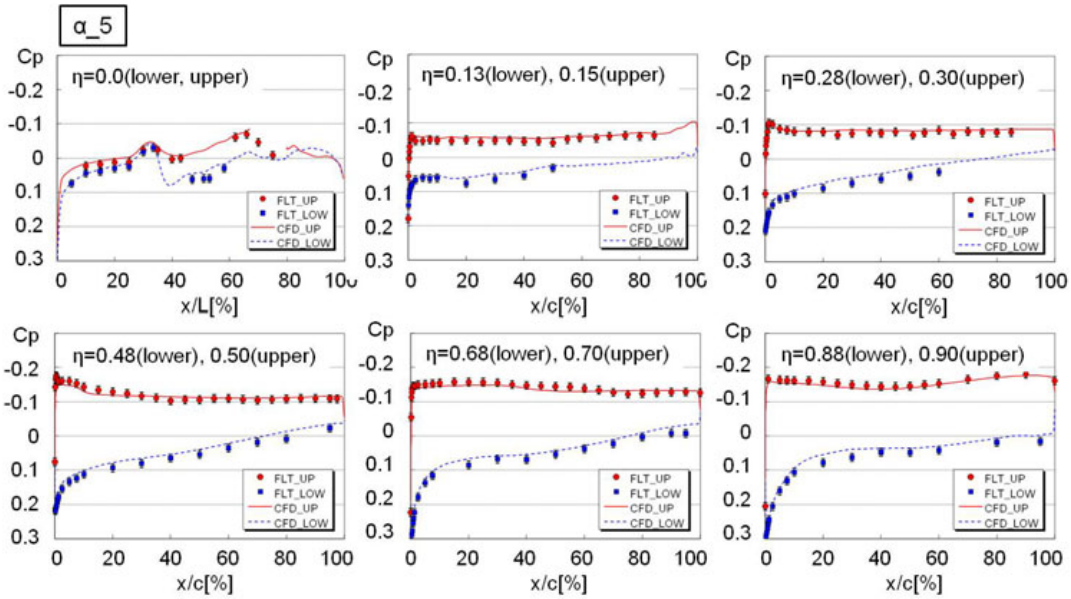

Fig.A-1(e) Comparison of Cp distributions at α _5

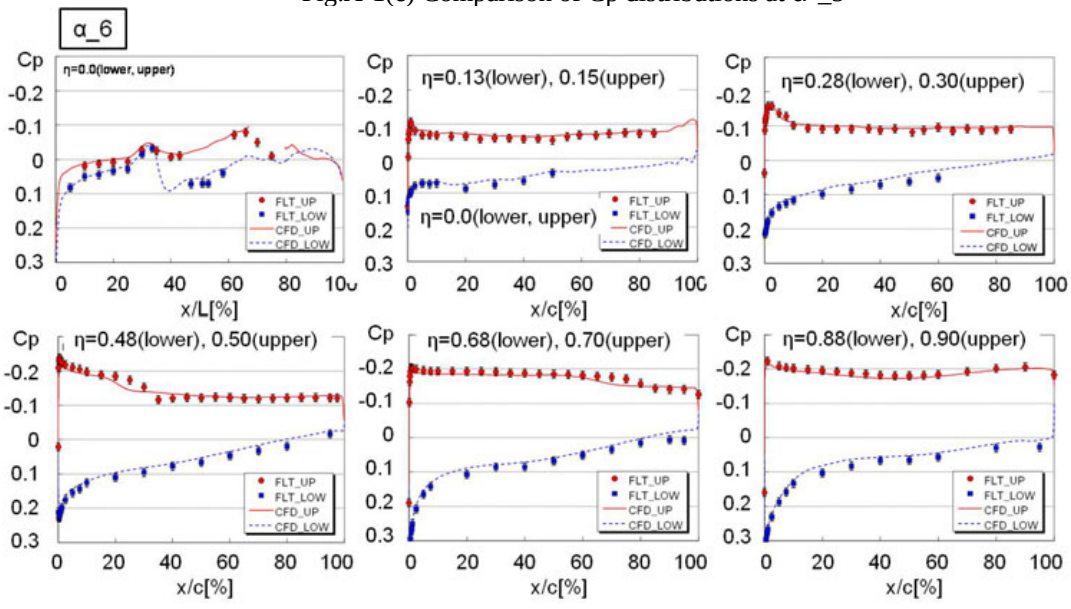

Fig.A-1(f) Comparison of Cp distributions at α _6

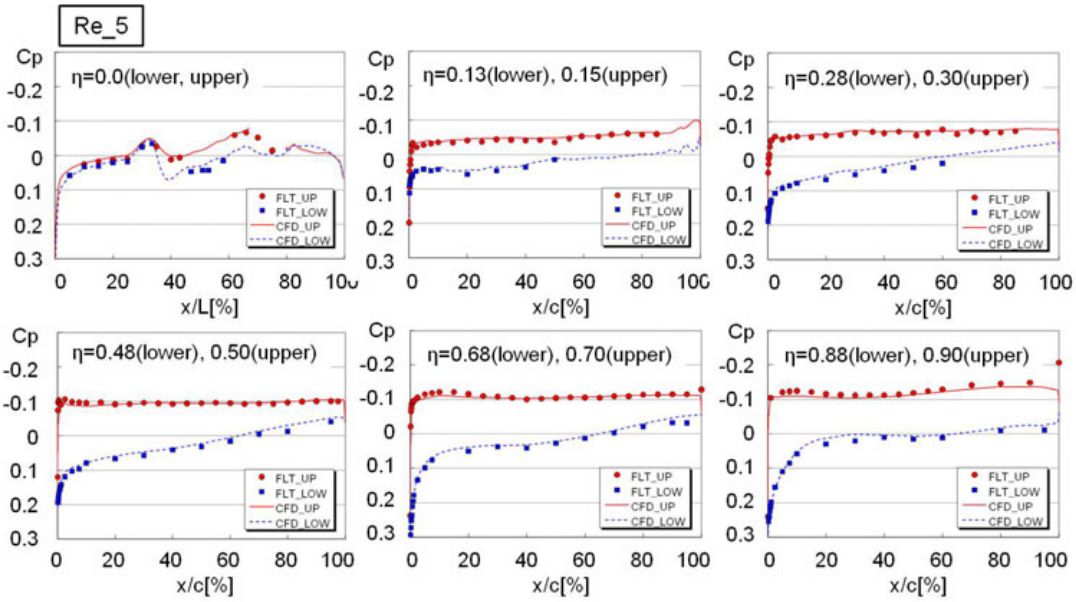

Fig.A-1(g) Comparison of Cp distributions at Re_5

Appendix B. Summary of Measured Transition Data

Fig. B-1(a), B-1(b), and B-1(c) show time histories of measured signals of representative DP, Pr, and TC sensors.

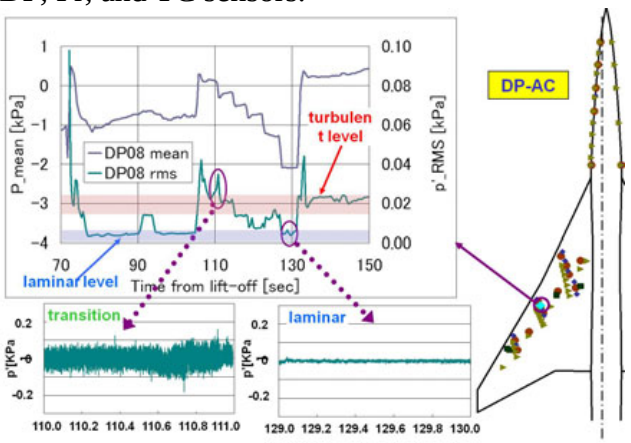

Fig.B-1(a) Time history of DP signals

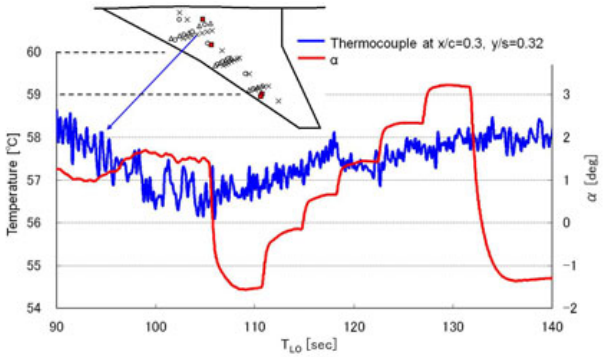

Fig.B-1(c) Time history of TC signals

Here, TC signal had relatively higher noise level due to present inherent electric circuit system. However, if the slope of averaged value is focused, the remarkable change of it roughly gives us any transition information.

Measured transition patterns over the wing and body are summarized in Fig. B-2(a) to 2(g).

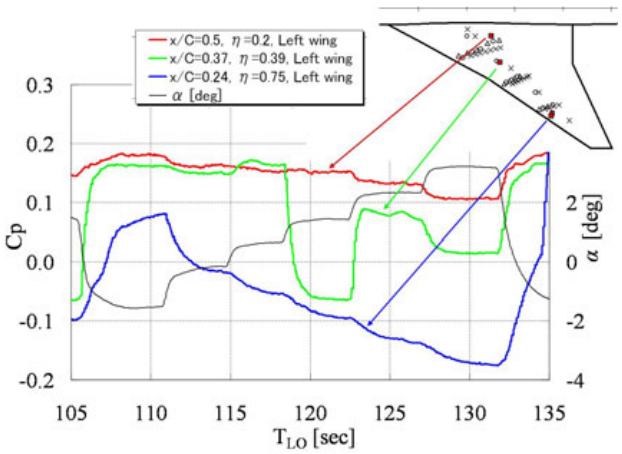

Fig.B-1(b) Time history of Pr signals

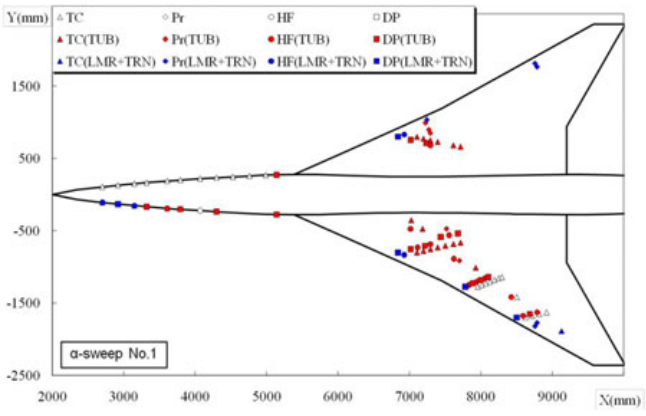

Fig.B-2(a) Transition pattern at α _1

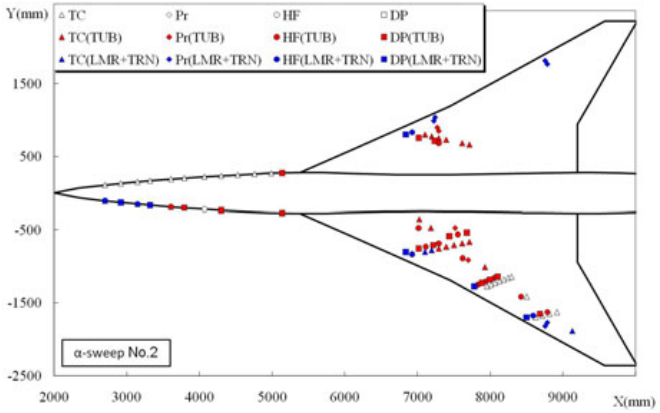

Fig.B-2(b) Transition pattern at α _2

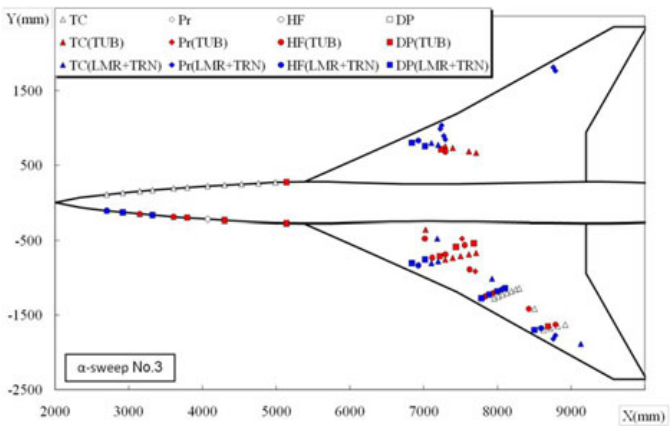

Fig.B-2(c) Transition pattern at α _3

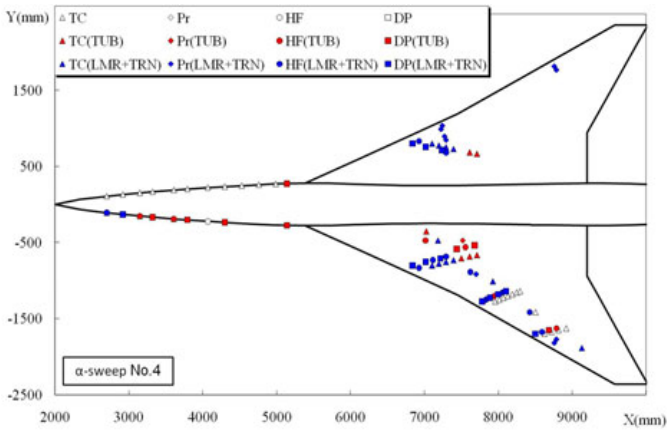

Fig.B-2(d) Transition pattern at α _4

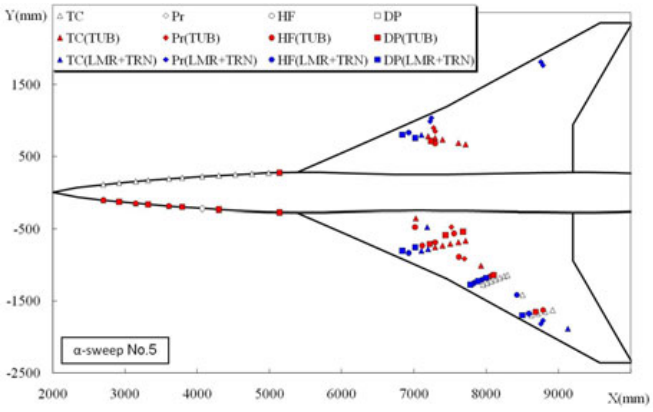

Fig.B-2(e) Transition pattern at α _5

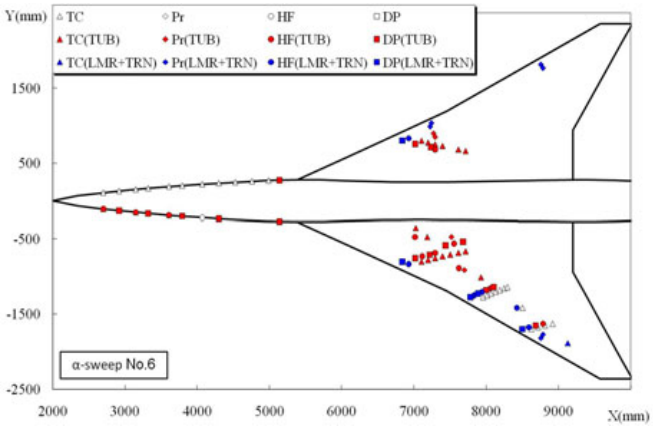

Fig.B-2(f) Transition pattern at α _6

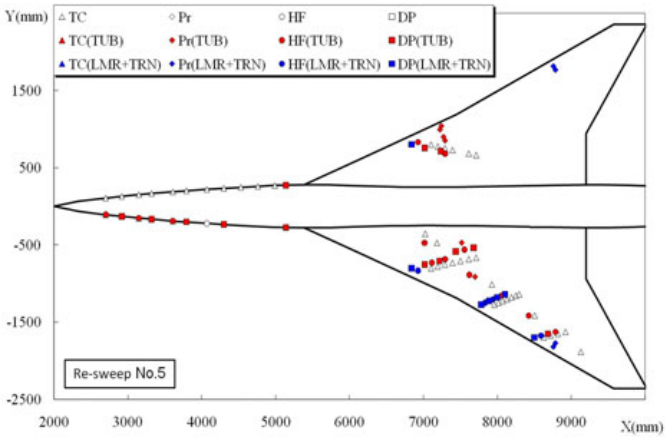

Fig.B-2(g) Transition pattern at Re_5